Development of Thermal Mapping System for Evaluating Protein Denaturation by Opposite-Phase Ultrasonic Scalpel

Yukiko KAWASUMI[1], Shunsuke MORIKAWA[1], Zhongwei JIANG [1], Minoru MORITA[1]
[1]Department of Mechanical Engineering, Yamaguchi University, Japan
d005wcu@gmail.com, mmorita@yamaguchi-u.ac.jp

Abstract: In this study, thermal denaturation sites in endovascular coagulation were evaluated using an opposite-phase vibration type ultrasonic coagulation and dissection device capable of inducing both longitudinal and bending vibrations. Since estimating thermal damage through temperature distribution is an effective approach for assessing coagulation performance, a dedicated experimental system was developed to capture the target temperature distribution. This enabled the visualization and analysis of the thermal denaturation areas. Image analysis using ImageJ was employed to quantify the regions discolored due to cumulative thermal exposure, indicative of protein denaturation.

Key-Words: *Ultrasonic Scalpel, Temperature Distribution, Measurements, Protein Denaturation*

1. Introduction

Endoscopic surgery is a minimally invasive technique to reduce the physical burden on patients undergoing operations for malignant neoplasms, cardiovascular diseases, and other conditions that currently represent major causes of mortality. This research focuses on the ultrasonic coagulation and dissection device, which is frequently employed in surgical operations. In contrast to conventional open surgery, which requires a large abdominal incision, endoscopic surgery is performed through several small incisions. The ultrasonic coagulation and dissection device, employed in endoscopic surgery, is designed to coagulate and dissect tissue using ultrasonic vibration. The advantages of this device are that it does not produce smoke, causes minimal tissue injury, is safe for the surgeon and patient, and facilitates dissection (Amaral, 1994).

The operating principle of the ultrasonic coagulation and dissection device involves converting high-frequency electrical energy into mechanical ultrasonic vibrations, generating high-frequency ultrasonic vibrations in the longitudinal direction. These ultrasonic vibrations break the tertiary structure of proteins by disrupting hydrogen bonds, causing the proteins to denature into a sticky coagulum (Amaral, 1994). As a result, blood vessels are sealed, achieving a hemostatic effect. Additionally, the frictional heat generated as a secondary effect further promoted coagulation. The vibrational frequency of the blade was approximately 55,500 cycles/second. This causes a knife-like action of the blade through tissue, with enough heating to create coagulation of small vessels (Lee and Park, 1999). Protein denaturation occurs at approximately 63℃, and unlike electrocautery or lasers, this method does not cause tissue carbonization or eschar formation (Dokiya, 2013). Although ultrasonic coagulation and dissection devices are recognized for their safety and effective coagulative performance, a standardized and widely accepted quantitative method to assess the relationship between thermal denaturation and temperature

Received: 2025/07/16, Accepted: 2025/12/08
*Corresponding author: Yukiko Kawasumi
E-mail address: d005wcu@gmail.com

distribution in actual biological tissues has not yet been fully established.

Therefore, this paper focuses on the development of an 'ultrasonic coagulation and dissection device' combined with an 'experimental setup for quantitatively evaluating thermal denaturation (using non-contact thermal imaging and tensile testing)'. This apparatus offers extensibility and utility for experimental research in this field. In previous studies, mechanical properties such as tensile tests on biological tissues have been evaluated; however, there are few reports on mechanical evaluations of coagulated and adhered tissues. Furthermore, this study aimed to evaluate the tissue that has undergone thermal denaturation by an ultrasonic scalpel, using tensile testing on the intimal layer of blood vessels. Moreover, during the coagulation process, the heat applied to the blood vessel was monitored using a thermal camera, and the resulting temperature distribution was recorded. By comparing this distribution with the area of discoloration on the vascular endothelium, the relationship between thermal exposure and coagulative denaturation is investigated. Accurate assessment of thermal denaturation in blood vessels is challenging due to variations in the output of the ultrasonic coagulation and dissection device as well as individual differences in the vascular endothelium. However, if denaturation can be consistently identified at a specific temperature under controlled conditions, regardless of differences in output or irradiation time, it may be possible to establish a threshold for determining the onset of denaturation. One method for measuring tissue temperature is the contact method using a thermocouple (Koch et al., 2003). In contrast, infrared temperature measurement offers the advantages of non-contact operation and the ability to quantitatively capture two-dimensional temperature distributions (Ota, 2006).

In this study, a thermal camera (FLIR, T530 Macro) was used to measure the temperature rise during the application of the ultrasonic scalpel. As shown in Fig.1 (left), conventional temperature measurement with a thermal camera focused on detecting the maximum surface temperature of the vascular endothelium during pressing experiments to evaluate heating performance under anti-phase vibration. In this study, however, to compare the vascular deformation with the temperature distribution, the camera was aligned parallel to the vessel surface, as shown in Fig.1(right). The covered region was exposed using an ultrasonic scalpel, allowing more precise measurement from a closer and perpendicular position to the endothelium. Furthermore, by measuring two overlapping vessels from the reverse side, we examined the temperature required for both denaturation and adherence.

This paper aimed to establish a method for evaluating the performance of ultrasonic coagulation and dissection devices by examining the relationship between temperature distribution and tissue degeneration based on the results of experiments using this method.

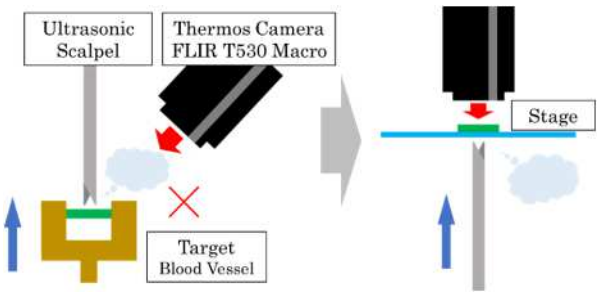

Fig.1 Orientation of the ultrasonic scalpel and the direction of the thermal camera in the previous study (left) and in the current experiment (right).

2.Configuration of experimental setup

In this study, to evaluate the thermal coagulation performance and adhesive strength of tissue using an ultrasonic coagulation and dissection device, we constructed an experimental setup that could consistently perform heating, temperature measurement, and tensile testing on the vascular endothelium.

2.1 Equipment Overview and Design Concept

This section describes the overall structure of the experimental setup constructed in this study and the arrangement of each component. There are four main features. Feature① serves as the introduction section, while Features② through ④ are described in detail below.-Figure 2 shows a front view of the entire device, showing the relative relationship between the load cell, ultrasonic scalpel, and slide mechanism. As shown in Figs.3-5, this apparatus primarily consists of the following components: Fig.3 shows the vascular fixation unit, and Figs.4 and 5 show the ultrasonic scalpel holder and press mechanism, respectively. Fig.2 shows the load cell (Yamaden, RE2-33005C) that measures the pressing load, and the thermal camera observation part that measures the temperature. An endovascular fixation section was ble pressing and heating conditions. mounted on the top of the device via an XY stage, allowing fine adjustment in the X and Y directions to precisely align the tip of the scalpel with the center of the vascular endothelium. The design of this fixture allowed for highly reproducibility.

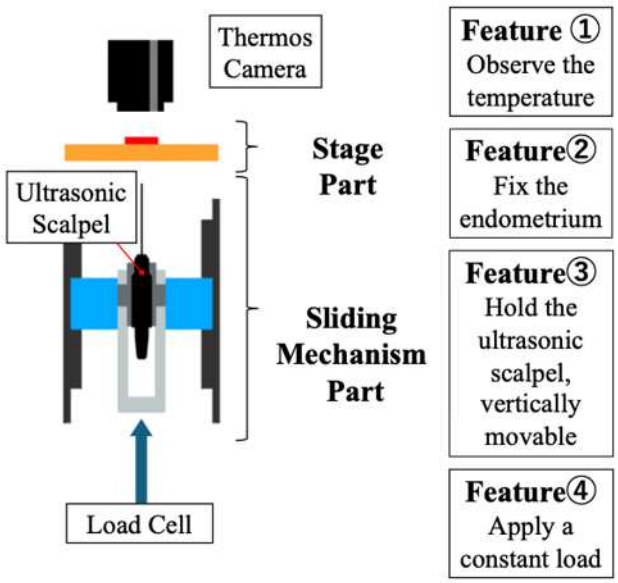

Fig.2 Front view of experimental apparatus

The temperature increase was measured non-contact by a thermal camera through an aperture in the upper part of the device, and the two-dimensional temperature distribution of the heated area was obtained. The ultrasonic scalpel was mounted on a slide mechanism below the device and could be moved vertically. It was installed on a load cell to measure the pressing load in real time.

2.2 Details of each part structure and function

2.2.1 Mechanism of vascular endometrial fixation (Feature②)

As shown in Fig.3, the vascular endothelium is fixed by a customized jig consisting of two parts: (1) the lower part of the clamping plate, (2) the upper part of the clamping plate. They were fabricated using a 3D printer and designed to stably sandwich the endosteum from the top and bottom. An aperture for temperature measurement was provided at the center, which was directly visible from the thermal camera. The entire fixation mechanism is mounted on an XY stage, which allows fine adjustment in the X and Y directions and is designed to enhance the accuracy of alignment between the vascular endothelium and the scalpel tip. The adjustment mechanism is orthogonal to the working direction (pressing direction), making it easy to ensure a reproducible test position.

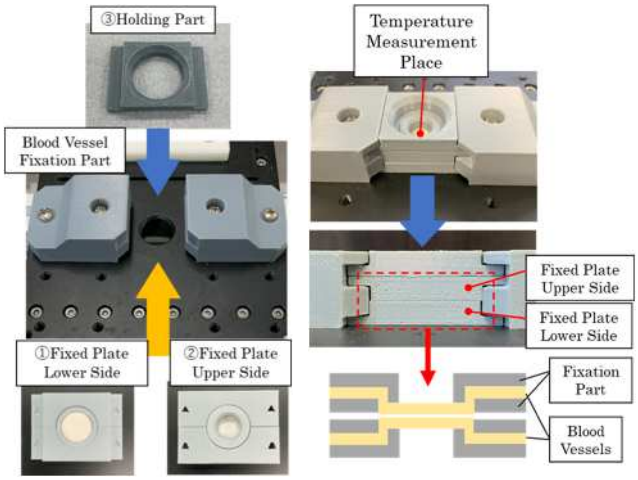

Fig.3 Experimental apparatus (left: inner membrane fixation part, center: temperature measurement part and fixation on the stage, right: stage part)

2.2.2 Ultrasonic scalpel holding mechanism and Slide mechanism（Feature③）

The handle of an ultrasonic scalpel has an ergonomically complex shape, and its retention requires components tailored to the individual shape. In this study, the handle of a scalpel was scanned using a 3D scanner, the shape of the holding part was modeled in 3D, and a matching holding fixture was created using a 3D printer (Figure 4, right). This holding section was attached to a slide mechanism and could move in a straight line in the vertical direction. This enables experiments that also consider changes in heat transfer and solidification area depending on the pressing angle. As shown in Figure 5, the slide mechanism uses a rail and bearing slider to ensure stable vertical motion.

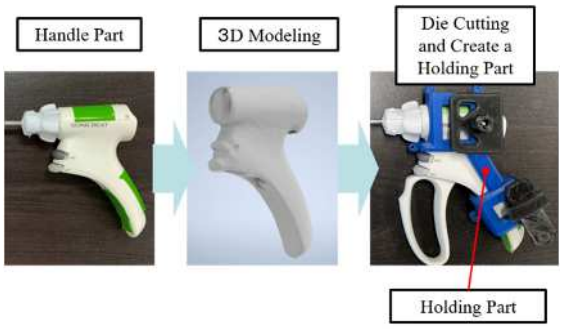

Fig. 4 Ultrasonic scalpel holding part

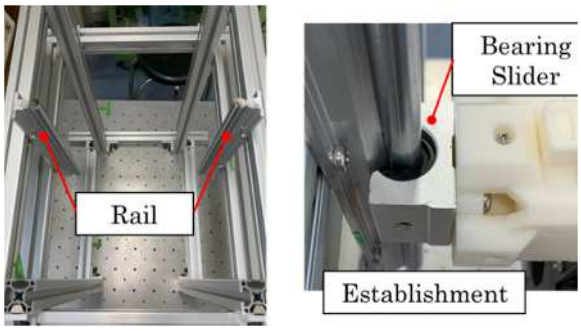

Fig. 5 Slide mechanism part

2.2.3 Load measurement system（Feature④）

As shown in Fig.2, the holder and load cell were integrated into the slider, and the load at the time of pressing was measured with high accuracy by the load cell under the holder. To confirm the reproducibility of the pressing load, a small load cell (FS10:UCW2) was installed in the vessel placement area, as shown in Fig.6, before the experiment to measure the load in advance. The effectiveness of the experimental setup was confirmed by setting the pressurization conditions for the reproduction experiment.

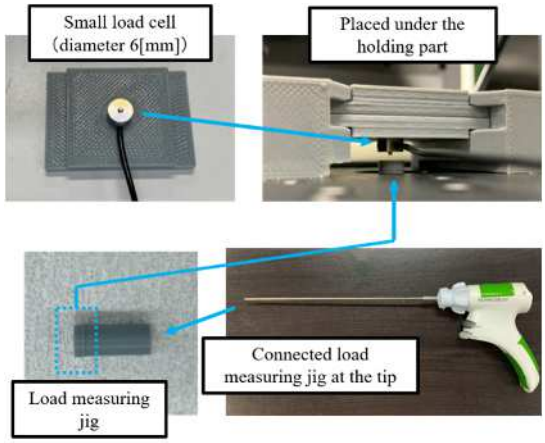

Fig. 6 Small load cell and load measuring jig

3. Experimental Methods

This study involved developing an experimental setup to evaluate the thermal coagulation performance and adhesive strength of an ultrasonic coagulation and dissection device. This system facilitates the integrated heating, temperature measurement and tensile testing of vascular endothelium. This chapter outlines the materials employed, the testing process, and the conditions applied.

3.1 Previous studies on mechanical characterization of biological tissues

Uniaxial compression and tensile tests are widely used to evaluate the mechanical properties of biological tissues. The effectiveness of tensile tests, particularly for vascular tissues, has been demonstrated in numerous studies.（Camasão and Mantovani, 2021 ; Qi et al., 2018 ; Kasyanov et al., 2011 ; Laterreur et al., 2014 ; Huh et al., 2019 ; Butlin et al., 2020）Burst and ring tensile tests have also been used to evaluate the structural strength of vessel walls (Laterreur et al., 2014), and in particular, Huh et al. performed uniaxial tensile tests on

porcine aorta to determine deformation behavior and fracture characteristics (Huh et al., 2019).

Although all of these studies were conducted on untreated biological tissues, there have been very few quantitative evaluations of the mechanical strength of adhesively bonded tissues by thermal coagulation.

In this study, we performed tensile tests on bovine endothelium coagulated using an ultrasonic scalpel in order to evaluate adhesion formation and strength.

3.2 Preparation of Specimens and Experimental Setup

As shown in Fig.7(a), frozen bovine aortas were thawed and the inner membrane, which was approximately 1 mm thick, was peeled off. The amount of water, which affects the stability of adhesion, was adjusted by injecting 0.02 mL of water between the inner membranes, and the experiments were conducted under constant wetting conditions. This is intended to promote cavitation and maintain constant heating efficiency by ultrasonic waves. (Payne Jr., 1994 ; Hachiya et al., 2012) As shown in Fig.7(b), the inner membrane was clamped from the top and bottom by a special fixing plate and placed in the experimental setup in a precisely aligned position. Prior to the solidification experiment, it was confirmed in advance that the pressing load reached each condition using the small load cell (FS10:UCW2) described in the previous chapter.

3.3 Coagulation and heating experiments and tensile testing

As shown in Fig.7(c), the ultrasonic coagulation and dissection device was pressed vertically toward the endothelium of the vessel from below the stage. The pressing speed was 0.1 mm/s. When a predetermined load was reached, a current of 0.3 A was applied for 30 seconds for coagulation. For the 2 N condition, an additional heating time of 40 seconds was also set.

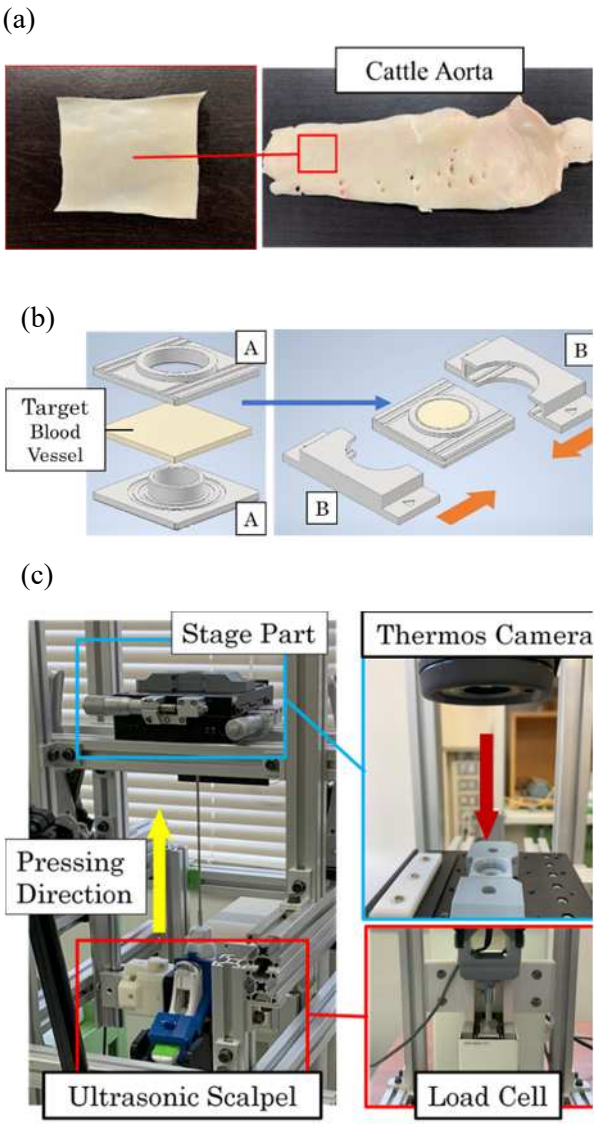

Fig. 7 The left figure in (a) shows the intimal portion of a Cattle aorta, cut into approximately 0.5 mm thicknesses. (b) shows the fixation panel that clamps the target vessel, (A) shows how to clamp a 0.6mm vessel, and (B) shows how to fix the vessel clamped using (A). (c) shows the ultrasonic scalpel being pressed against the stage section from the bottom.

The temperature distribution during heating was measured by a thermal camera in a non-contact manner. After coagulation, a uniaxial tensile test was performed. The upper fixture was connected to the tensile jig of a creep meter, and the tensile load was measured by moving the lower load cell at a constant speed. The tensile speed was 0.1 mm/s.

After coagulation, the inner membrane was wrapped in Kimwipes to keep it moist and retain moisture until testing. In the tensile test, adhesion was

considered successful as cases where the initial value at the start of the test, measured using the dedicated software for the RE2-33005C load cell, exceeded 0.03N.

3.4 Organization of experimental conditions

The following is a summary of each condition in this experiment.

Pressing speed: 0.1 mm/s

Pressing load: 2 N, 3 N, 4 N

Heating current: 0.3 A

Heating time: 30 s (also 40 s for 2 N condition only)

Moisture adjustment: 0.02 mL water added between inner membranes

4. Results

4.1 Maximum temperature measurement results

The results of the maximum temperature obtained in the experiment are shown in Figs.8(a)-(d) for each condition of pressing load and current application time. The maximum temperature values were extracted and plotted from the temperature trends recorded by the thermal camera during the heating process. Fig.8(a) shows the results under a 2 N load with a current applied for 30 seconds, while Fig.8(b) shows the same load with a 40-second current application. Fig.8(c) shows 3N and 30 seconds, and Fig.8(d) shows 4N and 30 seconds. As shown in Fig.8(a), the temperature peaked at approximately 150°C under the 2 N, 30 s condition. On the other hand, Fig.8(b) confirms that extending the current application time to 40 seconds at the same 2 N load resulted in a temperature increase to between 250°C and 300°C. In Fig.8(c) (3N, 30 sec) and Fig. 8(d) (4N, 30 sec), the temperatures reached higher than 250°C in both cases. These results indicate that the heating temperature tends to increase significantly when the pressing load is high, or the electric current duration is long. A total of 28 datasets were obtained across four experimental conditions, serving as a robust foundation for subsequent evaluations of thermal denaturation behavior.

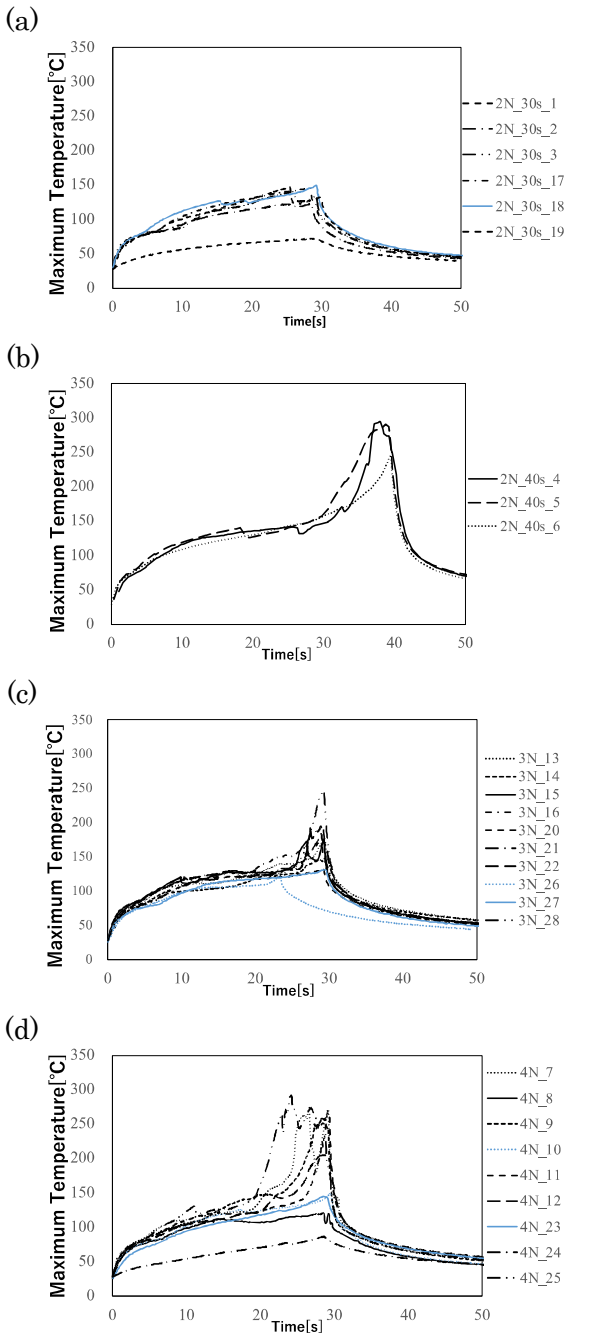

Fig. 8 The results in (a) and (b) correspond to the time variation of the maximum temperature for the experiments performed at 2N for 30 seconds and 2N for 40 seconds, respectively. The results in (c) and (d) correspond to the time variation of the maximum temperature for the experiments performed at 3N and 4N, respectively.

4.2 Comparison of discolored areas and cumulative temperature

Among the 28 experimental datasets obtained, thermal discoloration of the vascular endothelium—used as a visual indicator of protein denaturation—was clearly observed in 14 cases. These 14 datasets were selected for

further analysis of cumulative temperature distributions along the denaturation contours. To investigate the relationship between thermal denaturation and cumulative temperature, the cumulative temperature values (°C·s) were extracted along the contours of the discolored areas for each of the 14 cases. These contours were obtained by drying the samples for two days after coagulation, during which the denatured regions appeared as white discoloration. As shown in Fig.9, the post-drying images were binarized using ImageJ to extract the contours of the discolored regions. Based on these contours, cumulative temperature maps were generated by integrating the pixel-wise temperature data obtained from thermal imaging over a 50-second period during the heating process.

To illustrate the measurement and analysis procedure, one representative result was selected from each of the four experimental conditions—(a) 2N–30s, (b) 2N–40s, (c) 3N–30s, and (d) 4N–30s—and analyzed in detail. In each representative case, five or six points were selected along the contour (excluding extremely hot areas, such as those directly under the blade tip), and the corresponding cumulative temperatures were extracted.

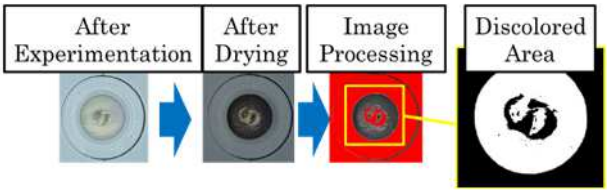

Fig.9 Post-experimental vascular intima after drying. The image was captured two days after the experiment, and the thermally discolored regions were extracted by binarization using image processing.

Fig.10 shows the binarized images of discolored regions (left column) and the corresponding cumulative temperature maps (right column), while the extracted cumulative temperatures are summarized in Table 1. In the temperature maps, white to yellow indicates high temperature ranges and blue to purple indicates low temperature ranges. The selected points are annotated with numbers. Furthermore, to statistically evaluate the

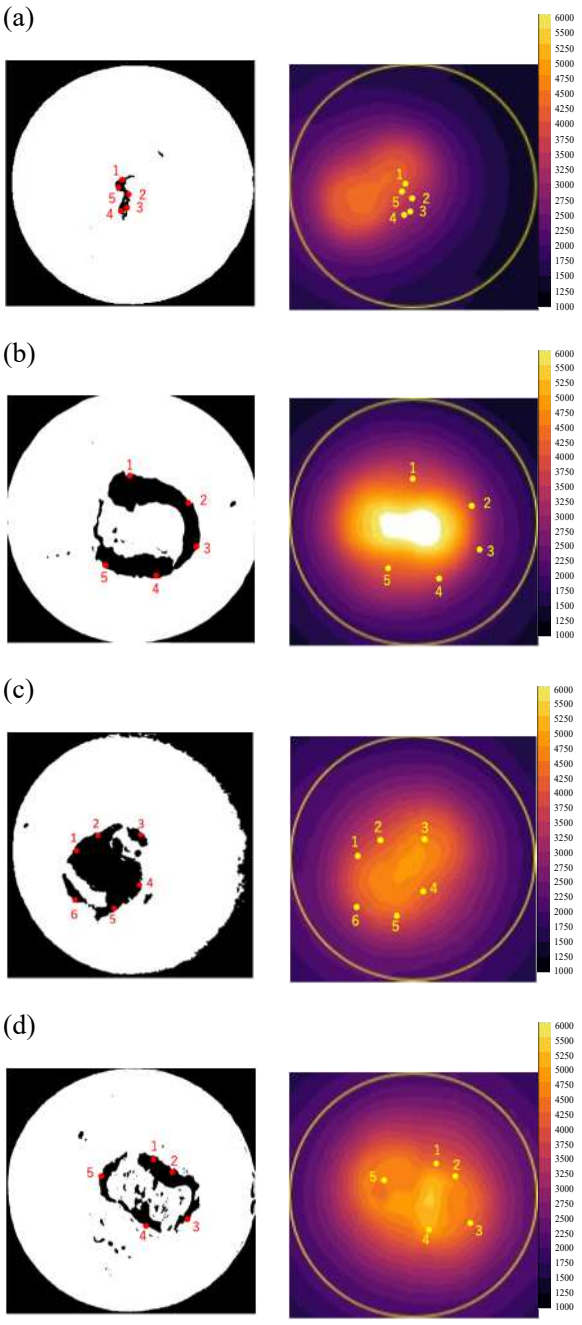

Fig.10 Representative results for each condition: 2 N–30 s (a), 2 N–40 s (b), 3 N–30 s (c), and 4 N–30 s (d). In each panel, the left image shows the binarized discoloration region after drying, and the right image shows the corresponding cumulative temperature map obtained from thermal imaging.

Table.1 Cumulative Temperature

Samples	2 N–30 s	2 N–40 s	3 N–30 s	4 N–30 s
1	4095	4602	4074	4764
2	3646	5416	4067	5048
3	3296	4978	4618	4597
4	3546	4565	4735	4946
5	3952	4296	4656	4715
6			4448	

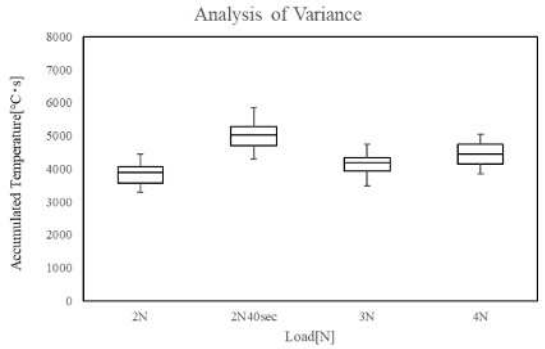

Fig.11 Box-and-whisker plots of cumulative temperature values along the discoloration contours under each load condition (2 N–30 s, 2 N–40 s, 3 N–30 s, and 4 N–30 s). T-tests and F-tests were performed to assess statistical differences.

cumulative temperature distribution across all 14 samples, the minimum, maximum, median, and interquartile range of the cumulative temperatures along the contours were analyzed for each condition.

Fig.11 presents the box-and-whisker plots of these distributions under the four conditions. The overall results show that cumulative temperatures at the discolored contours generally ranged from 3500 to 5500 °C·s, with relatively stable variation between conditions. The analysis of the 14 samples revealed that the average cumulative temperature along the discoloration contours was 4310 °C·s, with a 95% confidence interval of ±14.53 °C·s, indicating a relatively consistent threshold for thermal denaturation under controlled experimental conditions. This result suggests that cumulative temperature can serve as a reliable indicator of tissue denaturation.

5. Discussion

The results presented in Section 4.2 demonstrated that the average cumulative temperature along the discoloration contours was 4310 °C·s with a 95% confidence interval of ±14.53 °C·s, indicating a relatively consistent threshold for thermal denaturation under controlled conditions. However, it should be noted that this threshold was derived from the visible edges of the discolored regions and is therefore not necessarily the minimum value required to initiate denaturation. In fact, several data points within the full set of 14 samples exhibited cumulative temperatures approaching 5500 °C·s along the contours, suggesting that, depending on the thermal environment and experimental conditions, a significantly higher cumulative temperature may be required to induce denaturation. This highlights the importance of considering variability in tissue response and spatial temperature gradients when using cumulative temperature as an indicator for protein denaturation. Furthermore, while the use of discoloration contours provided a practical and reproducible method for assessing the extent of thermal denaturation, this approach inherently relies on visual changes in tissue appearance, which may not fully capture the molecular or structural transitions occurring at a microscopic level. The threshold derived from visual observation, though statistically consistent across controlled samples, may not universally represent the onset of protein denaturation across different tissue types or under varying hydration and mechanical conditions. In this context, the cumulative temperature should be regarded as a practical but empirical indicator that reflects the thermal history of the tissue rather than a strict biochemical threshold. The observed variation—ranging from approximately 3500 to 5500 °C·s—may be attributed to several factors, including slight differences in tissue thickness, initial water content, contact angle of the blade, and local variability in thermal conductivity. These elements collectively influence the heat distribution and, consequently, the point at which visible denaturation occurs. In addition, although the experimental setup enabled consistent control of pressing force and heating time, the spatial resolution of thermal imaging and the accuracy of image binarization could influence the extracted contour positions and the corresponding cumulative temperature values. It is therefore essential to validate the reliability of image-derived thresholds through additional methods, such as

histological staining or molecular markers, which can independently verify the occurrence of protein denaturation. Finally, for practical application in clinical or device design contexts, the integration of quantitative thermal evaluation with mechanical performance metrics—such as tensile strength or sealing efficacy—will be crucial. Establishing a comprehensive framework that connects cumulative temperature, tissue denaturation, and mechanical adhesion will facilitate the development of optimized ultrasonic treatment protocols that are both safe and effective.

6. Conclusion

In this study, we developed an experimental setup for the quantitative evaluation of thermal denaturation induced by a novel opposite-phase vibration ultrasonic coagulation and dissection device. By integrating non-contact thermal imaging with tensile testing, we successfully measured the temperature distributions during ultrasonic heating and assessed the corresponding tissue adhesion and denaturation effects. Through experiments conducted under four different loading and heating conditions, a total of 28 datasets were obtained, of which 14 showed clear thermal discoloration indicative of protein denaturation. This result, with a mean cumulative temperature of 4310 °C·s and a 95% confidence interval of ±14.53 °C·s, indicates a relatively consistent threshold for protein denaturation under the specified experimental conditions. However, variability in the observed cumulative temperatures—ranging from approximately 3500 to 5500 °C·s—underscores the influence of local tissue properties and environmental conditions on the heat-induced denaturation process. While the results confirm the utility of cumulative temperature as a practical indicator of thermal denaturation, they also highlight the limitations of relying solely on visual indicators, such as discoloration contours. To enhance accuracy, future studies should incorporate biochemical or histological validation. Furthermore, combining thermal distribution data with mechanical evaluation—such as tensile strength and adhesion integrity—will be essential for establishing comprehensive performance metrics for ultrasonic surgical devices. The experimental framework developed in this study provides a robust foundation for optimizing device parameters and treatment protocols. This study also opens the door to future exploration of tissue-specific thresholds and real-time thermal control, with the ultimate goal of improving the safety, efficacy, and predictability of ultrasonic coagulation in minimally invasive surgery.

Acknowledgment

This work was supported by JST SPRING, Grant Number JPMJSP2111. JSPSKAKWNHI, JP22K12866

References

[1]Amaral JF, "The experimental development of an ultrasonically activated scalpel for laparoscopic use," Surg Laparosc Endosc 4, 92-99, 1994

[2]Christian Koch, Thomas Friedrich, Frank Metternich, Andrea Tannapfel, Hans-Peter Reimann, Uwe Eichfeld; Determination of temperature elevation in tissue during the application of the harmonic scalpel; Ultrasound in Medicine & Biology Volume 29, Issue 2, Pages 301-309, 2003

[3]D.B.CamasãoD.Mantovani , The mechanical characterization of blood vessels and their substitutes in the continuous quest for physiological-relevant performances. A critical review, Materials Today Bio, Volume 10. 2021

[4]Dokiya, T., "Fundamentals of Ultrasonic Coagulation Cutting Devices and the Lifetime of Handpieces," Medical Instrumentation, Vol. 83, No. 3, pp. 317-320, 2013.

[5]Hachiya, H., et al., "Fundamental Study on Cavitation Generation in Ultrasonic Coagulation Cutting Devices," Ultrasonics in Medicine, pp. 110-111, 2012.

[6]J H Payne Jr, "Ultrasonic dissection," Surg Endosc. 1994 May;8(5):416-8.

[7]Jingjing Yang, Benyang Rong, Lei Wang, Minoru Morita, Guifang Deng, Yifan Jiang and Junbing Qian, Analysis and Structure Optimization of Scissor-Type Micro-Stirrer with the Most Effective Output Performance for

Thrombus Dissolution in Interventional Therapy,Actuators 2023,12(2),No.60,pp1-19,2023.

[8]Jingjing Yang, Minoru Morita, Zhongwei Jiang; Design of a novel scissoring micro-stirrer for blood clot dissolution; Sensors and Actuators A: Physical , Volume248, pp.130-137, 2016.

[10]Ji Qi, MD, Shaoqun Zhang, MD, Lei Zhang, MD, Ruiyue Ping, MM, Kaike Ping, MM, Da Ye, MB, Honggui Shen, MM, Yili Chen, MM, Yikai Li, MD, PhD, Uniaxial Tensile Properties of Atherosclerotic Carotid Artery After Mobilization of Pushing on Qiao-Gong: A Safety Study Using an Animal Model of Carotid Atherosclerosis , Journal of Manipulative and Physiological Therapeutics, Volume 41, Issue 2, pp164-173, 2018.

[11]Mark Butlin, Isabella Tan, Bart Spronck, Alberto P. Avolio , Measuring Arterial Stiffness in Animal Experimental Studies, Arteriosclerosis, Thrombosis, and Vascular Biology, Vol.40, No.5, pp1068‐1077, 2020.

[12]Minoru Morita, Jingjing Yang, Zhongwei Jiang, Advances in Endovascular Intervention Using Biomaterials: Study on Heat Efficiency of Scissor-Type Ultrasonic Catheter Device, BioMed Research International, Vol.2021,15 Pages 3.10.2021.

[13]Minoru MORITA, Shunsuke MORIKAWA, Zhongwei JIANG,Development of invitro blood vessel coagulation-incision experimental method and characterization of opposite-phase vibration type ultrasonic scalpel,The Journal of Advanced Mechanical Design,Systems, and Manufacturing(JSME),Volume 17 Issue 4,2023.

[14]Minoru Morita, Jingjing Yang, Zhongwei Jiang, Study on heat efficiency of scissor-type ultrasonic catheter device, BioMed Research International, vol. 2021, Article ID 5543520, 15 pages, 2021.

[15]Mohammad A joudanian, Zhongwei Jiang and Minoru Morita, Structural analysis and design of micro-stirrer driven at a requested frequency for thrombus dissolution,International Journal of Applied Electromagnetics and Mechanics.,Vol.41,No.1, pp87-96,2013.

[16]Ota, J., "Measurement Techniques Using Infrared Thermography," Journal of Electronics Packaging Society, Vol. 9, No. 6, pp. 446-450, 2006.

[17]Sang Joon Lee and Ki Hyun Park; Ultrasonic energy in endoscopic surgery; Yonsei Medical Journal, pp. 545-549, 1999.

[18]Sugimoto, O., "Objective Evaluation of Image Quality," The Institute of Electronics, Information and Communication Engineers, "Knowledge Forest," 2nd Group, 5th Edition, Chapter 9, -9-2, 2013.

[19]Up Huh, Chung-Won Lee, Ji-Hun You, Chan-Hee Song, Chi-Seung Lee, Dong-Man Ryu, Determination of the Material Parameters in the Holzapfel-Gasser-Ogden Constitutive Model for Simulation of Age-Dependent Material Nonlinear Behavior for Aortic Wall Tissue under Uniaxial Tension, Applied Sciences, Volume 9, Issue 14, 18 pages, 2019.

[20]Uetake, K., Yoshikawa, H., Yamaguchi, K., "Objective Evaluation Method Validation for Computer-Synthesized Holograms," Technical Report of the Institute of Image Information and Television Engineers, Vol. 41, No. 31, 2017.

[21]Uetake, K., Yoshikawa, H., Yamaguchi, K., "Study on Objective Evaluation Method of Computer-Synthesized Holograms Using Structural Similarity," Technical Report of the Institute of Image Information and Television Engineers, Vol. 40, No. 29, 2016.

[22]Véronique Laterreur, Jean Ruel, François A. Auger, Karine Vallières, Catherine Tremblay, Dan Lacroix, Maxime Tondreau , Jean-Michel Bourget , Lucie Germain, Comparison of the direct burst pressure and the ring tensile test methods for mechanical characterization of tissue-engineered vascular substitutes, Journal of the Mechanical Behavior of Biomedical Materials, Volume 34, pp253-263, 2014.

[23]V. Kasyanov, K. Brakke, T. Vilbrandt, R. Moreno-Rodriguez , A. Nagy-Mehesz , R. Visconti , R. Markwald , I. Ozolanta , R.A. Rezende , A.L. Lixandrao Filho, P. Inforc¸ati Neto, F.D.A.S. Pereira, D.T. Kemmoku, J.V.L. da Silva and V. Mironov, Toward organ printing: Design characteristics, virtual modelling and physical prototyping vascular segments of kidney arterial tree, Virtual and Physical Prototyping, Vol. 6, No.4, pp197.